

TIME-DEPENDENT MESOSCOPIC MODELLING OF MASONRY USING EMBEDDED WEAK DISCONTINUITIES

B. VANDOREN^{*†}, K. HEYENS^{*} AND K. DE PROFT[†]

^{*}XIOS Hogeschool Limburg
Departement TIW, Vakgroep Bouwkunde
Agoralaan Gebouw H, 3590 Diepenbeek, Belgium
e-mail: bram.vandoren@xios.be

[†]Hasselt University
Faculteit WET, Vakgroep FYS
Agoralaan Gebouw D, 3590 Diepenbeek, Belgium

Key words: masonry, mesoscopic modelling, weak discontinuities, partition of unity

Abstract. In this contribution, a rate-dependent mesoscopic masonry model is presented in which the mortar joints are incorporated by embedded weak discontinuities based on partitions of unity. Within the discontinuities, both an isotropic damage and a Perzyna viscoplastic model are used to describe joint degradation. The elastic domain of the joint behaviour is bounded by a modified Drucker-Prager yield function. The performance of the developed masonry model is demonstrated by the simulation of a three-point bending test and a shear wall test.

1 INTRODUCTION

The modelling of masonry has been a popular topic within computational mechanics for some years now. Two major groups of modelling approaches can be distinguished: macroscopic and mesoscopic [1]. In the macroscopic approach the joints and bricks are homogenized to one orthotropic material. The main advantage of this method is that not much computational effort is needed to calculate large structures. However, the obtained crack path is less detailed. This drawback can be alleviated by the use of mesoscopic models. In this approach, joints and bricks are modelled by separate entities. Classically, the joints are incorporated by interface elements, situated on the boundaries of the continuum brick elements [1, 2]. When a critical state is reached in a joint, a strong discontinuity (i.e. a jump in the displacement field) is introduced in the interface.

An alternative way to incorporate strong discontinuities is the partition of unity method [3, 4, 5]. Within this method, nodes are locally enhanced to enrich the solution with discontinuous modes. This concept was applied to masonry by De Proft et al. [6] and will be extended in this paper by the incorporation of weak discontinuities. A weak discontinuity introduces a jump in the strain field, allowing for failure to localise in a zone with finite width [7, 8, 9]. The thickness of this failure is in this case linked to the joint thickness.

2 PARTITION OF UNITY CONCEPT FOR WEAK DISCONTINUITIES

2.1 Displacement decomposition

The displacement field of a body crossed by a weak discontinuity (Figure 1) is obtained by:

$$\mathbf{u} = \hat{\mathbf{u}} + H_{\Omega^w} \tilde{\mathbf{u}} \quad (1)$$

in which $\hat{\mathbf{u}}$ and $\tilde{\mathbf{u}}$ denote the regular and enhanced displacement field, respectively. H_{Ω^w} is a unit ramp function [10], defined by:

$$H_{\Omega^w} = \begin{cases} 0 & \text{if } \mathbf{x} \in \Omega^- \\ \frac{\xi - \xi^-}{\xi^+ - \xi^-} & \text{if } \mathbf{x} \in \Omega^w \\ 1 & \text{if } \mathbf{x} \in \Omega^+ \end{cases} \quad (2)$$

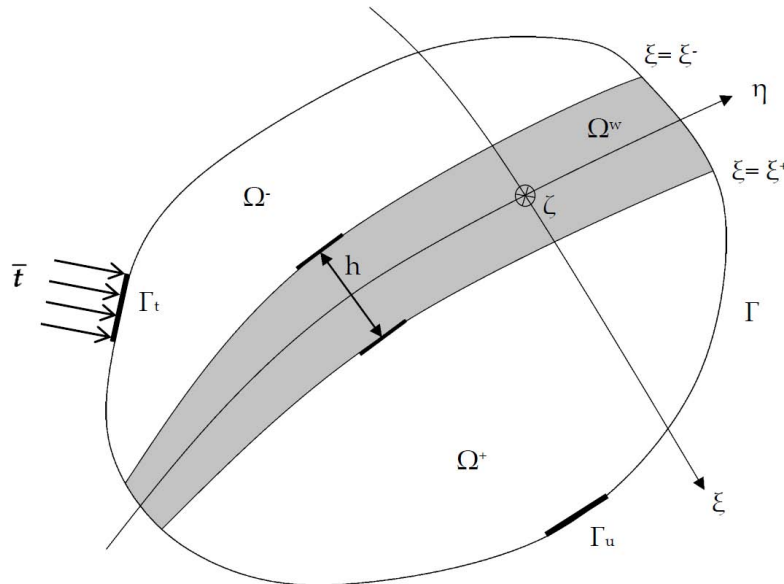


Figure 1: Body crossed by a weak discontinuity

2.2 GFEM discretisation

In this work, the Generalized Finite Element method has been adopted to model the discontinuities [11]. The unit ramp function (Equation (2)) is used as an enhanced basis: its value equals unity for a point inside a masonry brick. When a support of a node is crossed by a weak discontinuity (i.e. joint), an enhanced set of degrees of freedom is added to the solution field of that node. Consequently, each brick possesses its own set of enhanced degrees of freedom. Special care has to be taken in the implementation of a meshgenerator, to prevent linear dependency of the enhanced basis functions [11]. In the current model, two linear quadrilateral elements are used to model one brick.

3 MATERIAL MODELS

Two material laws have been implemented to model the nonlinear joint behaviour: an isotropic damage model and a viscoplastic model. The stone behaviour remains linear elastic throughout the simulations. Consequently, cracks cannot run through bricks.

3.1 Damage model

The nonlinear joint behaviour is governed by an exponential damage evolution law [12]:

$$\begin{cases} \omega = 0 & \text{if } \kappa < \kappa_0 \\ \omega = 1 - \frac{\kappa_0}{\kappa} \exp\left[-\frac{(\kappa - \kappa_0)}{\gamma}\right] & \text{if } \kappa \geq \kappa_0 \end{cases} \quad (3)$$

where $\kappa_0 = \frac{f_{t0}}{E}$ in which E represents the Young's modulus of the mortar joints. The loading function κ , expressed in terms of strain invariants, is derived from the Drucker-Prager model [13]:

$$\kappa = \alpha \frac{I_{1,\varepsilon}}{1 - 2\nu} + \beta \frac{\sqrt{J_{2,\varepsilon}}}{1 + \nu} \quad (4)$$

The material parameters α and β are chosen to fit the uniaxial tensile strength f_{t0} and uniaxial compressive strength f_{c0} :

$$\alpha = \frac{1}{2} \frac{f_{c0} - f_{t0}}{f_{c0}} \quad (5)$$

$$\beta = \frac{\sqrt{3}}{2} \frac{f_{c0} + f_{t0}}{f_{c0}} \quad (6)$$

Finally, the brittleness of response is governed by γ :

$$\gamma = \frac{G_{fI}}{l_c f_{t0}} - \frac{1}{2} \kappa_0 \quad (7)$$

where G_{fI} denotes the mode I fracture energy and l_c is a regularising equivalent length parameter.

3.2 Viscoplastic model

An alternative way to model the softening and failure behaviour of masonry is the use of a viscoplastic model. The incorporation of this type of model is twofold: time-dependent behaviour can be modelled (e.g. the creep phenomenon [14]) and the model has a regularising effect [15, 16]. In this work, the Perzyna overstress model has been adopted [17]. Classically, the strain rate is decomposed into an elastic and a viscoplastic strain rate:

$$\dot{\boldsymbol{\epsilon}} = \dot{\boldsymbol{\epsilon}}^e + \dot{\boldsymbol{\epsilon}}^{vp} \quad (8)$$

in which the viscoplastic strain rate for non-associative flow is expressed by:

$$\dot{\boldsymbol{\epsilon}}^{vp} = \frac{1}{\eta} \langle \phi(f) \rangle \mathbf{m} \quad (9)$$

where η represents the viscosity parameter, f is a yield function and $\mathbf{m} = \frac{\partial g}{\partial \boldsymbol{\sigma}}$ in which g is a viscoplastic potential. $\langle \phi(f) \rangle$ is defined as:

$$\langle \phi(f) \rangle = \begin{cases} \left(\frac{f}{\bar{\sigma}_0} \right)^N & \text{if } f \geq 0 \\ 0 & \text{if } f < 0 \end{cases} \quad (10)$$

in which $\bar{\sigma}_0$ is the initial yield stress and scalar N is a material parameter which equals 1 in the present study. The rate-independent and elastic cases can be recovered when η approaches 0 and ∞ , respectively. The elastic domain is bounded by a modified Drucker-Prager yield surface, expressed in terms of stress invariants $I_{1,\sigma}$ and $\sqrt{J_{2,\sigma}}$:

$$f = aI_{1,\sigma} + \sqrt{\chi^2 + J_{2,\sigma}} - b \quad (11)$$

where χ controls the hyperboloid character of the yield surface (Figure 2). The original Drucker-Prager cone is recovered by setting $\chi = 0$. If $\chi \neq 0$, the apex is smoothed and no special stress return-mapping algorithms are required [16]. The material parameters a and b are chosen to fit the uniaxial tensile and compressive strengths:

$$a = \frac{1}{\sqrt{3}} \frac{f_c - f_t}{f_c + f_t} \quad (12)$$

$$b = \frac{2}{\sqrt{3}} \frac{f_c f_t}{f_c + f_t} \quad (13)$$

The viscoplastic potential used in this paper is given by:

$$g = a' I_{1,\sigma} + \sqrt{\chi^2 + J_{2,\sigma}} \quad (14)$$

in which a' is expressed in terms of the dilatancy angle ψ [14]:

$$a' = \frac{\tan \psi}{\sqrt{9 + 12 \tan^2 \psi}} \quad (15)$$

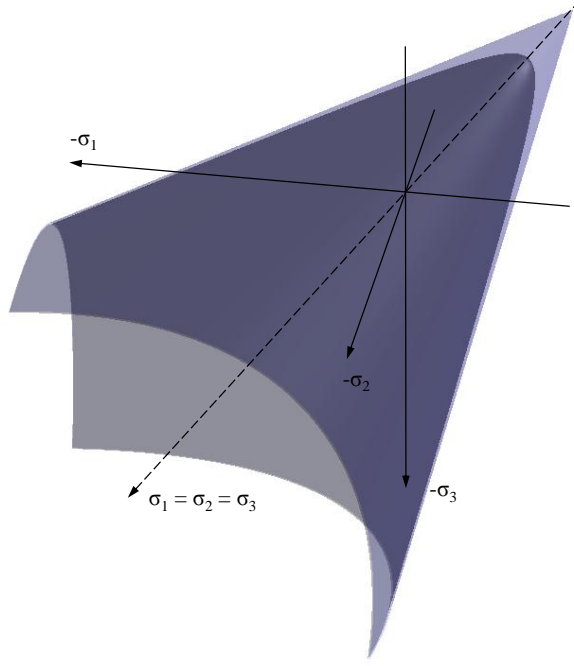


Figure 2: Drucker-Prager hyperboloid yield surface in principal stress space

Isotropic softening of the material model is determined by an exponential law:

$$f_t = f_{t0} \exp \left[-f_{t0} \frac{\kappa_w}{G_{fI}} \right] \quad (16)$$

where f_{t0} represents the initial uniaxial tensile strength and G_{fI} is the mode I fracture energy. In the present study, the compressive strength is assumed to remain constant during the simulations. The work softening parameter κ_w is calculated by:

$$\kappa_w = \Delta t \boldsymbol{\sigma}^T \dot{\boldsymbol{\epsilon}}^{vp} \quad (17)$$

in which Δt is the time increment. The viscoplastic rate equations are integrated with a fully implicit Euler backward scheme:

$$\begin{bmatrix} \mathbf{I} + \Delta \lambda \mathbf{D}^{el} \frac{\partial \mathbf{m}}{\partial \boldsymbol{\sigma}} & \mathbf{D}^{el} \bar{\mathbf{m}} \\ -\frac{\Delta t}{\eta} \frac{\partial \phi}{\partial f} \mathbf{n} & 1 - \frac{\Delta t}{\eta} \frac{\partial \phi}{\partial f} \frac{\partial f}{\partial \kappa_w} \frac{\partial \kappa_w}{\partial \lambda} \end{bmatrix} \begin{Bmatrix} d\boldsymbol{\sigma} \\ d\lambda \end{Bmatrix} = \begin{Bmatrix} \boldsymbol{\sigma}^{trial} - \boldsymbol{\sigma} - \Delta \lambda \mathbf{D}^{el} \mathbf{m} \\ \frac{\Delta t}{\eta} \langle \phi(f) \rangle - \Delta \lambda \end{Bmatrix} \quad (18)$$

where \mathbf{D}^{el} represents the elastic material stiffness matrix, $\mathbf{n} = \frac{\partial f}{\partial \boldsymbol{\sigma}}$, $\boldsymbol{\sigma}^{trial}$ denotes the elastic predictor stress and:

$$\bar{\mathbf{m}} = \mathbf{m} + \Delta \lambda \frac{\partial \kappa_w}{\partial \lambda} \frac{\partial \mathbf{m}}{\partial \kappa_w} \quad (19)$$

Since plane stress conditions are assumed in this paper, the return mapping procedure is performed in an expanded stress space ($\boldsymbol{\sigma} = \{\sigma_{xx} \sigma_{yy} \sigma_{xy} \sigma_{zz}\}^T$) and the zero out-of-plane stress condition $\sigma_{zz} = 0$ is enforced at integration point level [14, 18]. After the return mapping procedure, the algorithmic consistent tangent stiffness matrix is retrieved by:

$$\mathbf{D}^t = \mathbf{H} - \frac{\mathbf{H}\bar{\mathbf{m}}\mathbf{n}^T\mathbf{H}}{-\frac{\partial f}{\partial \kappa_w} \frac{\partial \kappa_w}{\partial \lambda} + \mathbf{n}^T\mathbf{H}\bar{\mathbf{m}} + \frac{\eta}{\Delta t} \frac{\partial \phi}{\partial \bar{f}}} \quad (20)$$

in which:

$$\mathbf{H} = \left((\mathbf{D}^{el})^{-1} + \Delta\lambda \frac{\partial \mathbf{m}}{\partial \boldsymbol{\sigma}} \right)^{-1} \quad (21)$$

4 NUMERICAL EXAMPLES

4.1 Three-point bending test

In order to demonstrate the potential of the developed mesoscopic masonry model, a three-point bending test has been carried out using the isotropic damage model. The material parameters are given by Tables 1-2. The results show a good agreement with the experimental data obtained from [19] (dotted curve).

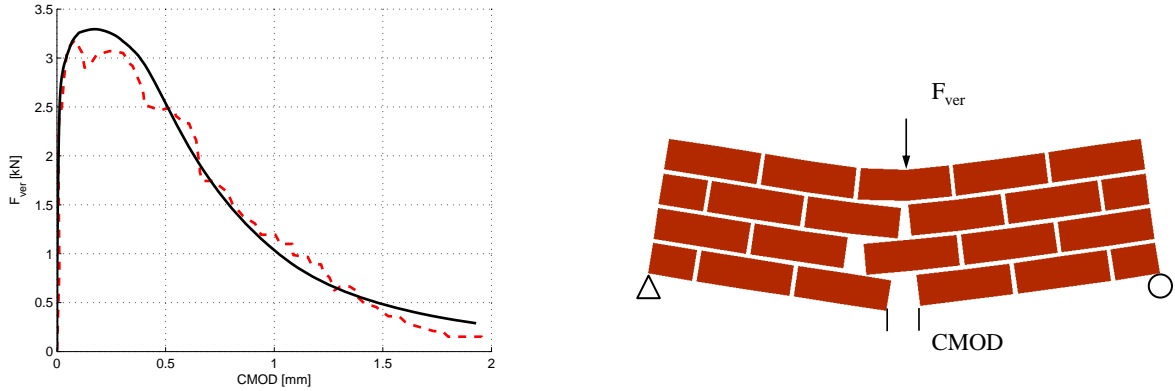


Figure 3: Load-CMOD curve and deformed mesh for a three-point bending test

Table 1: Elastic material parameters for the three-point bending test

	dimensions	E [N/mm^2]	ν
joints	10 mm	3369	0,20
bricks	$76 \times 230 \times 110$ mm ³	16700	0,15

Table 2: Inelastic material parameters for the three-point bending test

	f_{t0} [N/mm^2]	f_{c0} [N/mm^2]	G_{fI} [N/mm]	l_c [mm]
joints	0,086	7,26	0,002	1

4.2 Shear wall test

The second example is a shear wall with opening [20]. Tables 3-4 summarise the employed material parameters. A confining stress of $0,30 N/mm^2$ is applied on top of the wall. The average horizontal loading rate at the top equals $0,01 mm/s$.

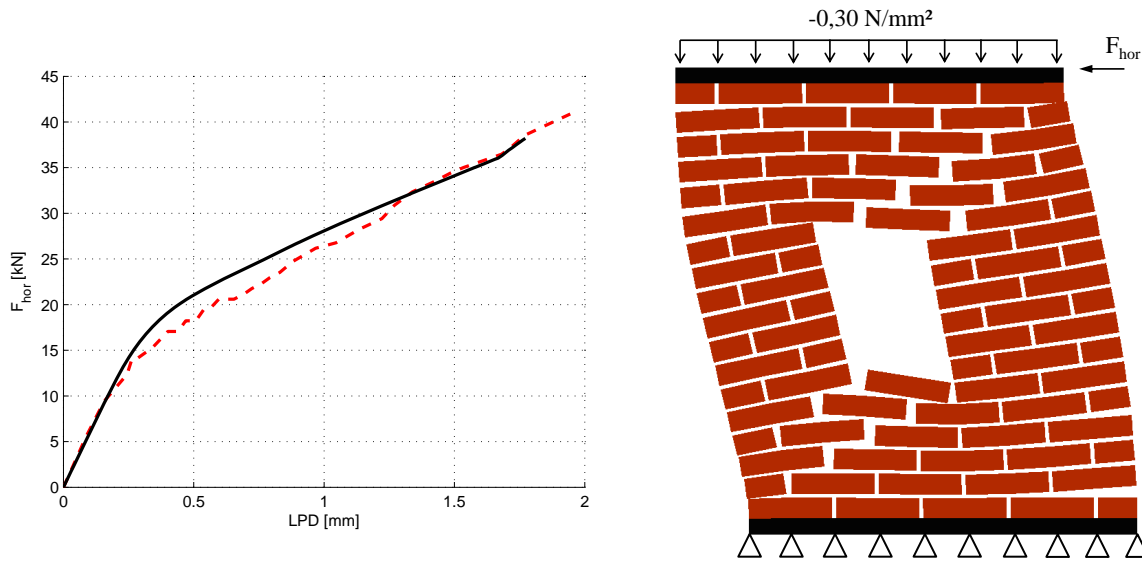


Figure 4: Load-displacement curve and deformed mesh for a shear wall test

The results show a good agreement with those from previous research work (dotted curve), in which a sequentially linear approach has been used [6]. Since no compressive cap is implemented, no compressive failure takes place and the load-displacement curve keeps increasing. The typical stair-step crack pattern, found in experimental tests [20], is recovered.

Table 3: Elastic material parameters for the shear wall test

	dimensions	E [N/mm^2]	ν
joints	10 mm	782	0,14
bricks	$52 \times 210 \times 100 mm^3$	16700	0,15

Table 4: Inelastic material parameters for the shear wall test

	f_{t0} [N/mm ²]	G_{fI} [N/mm]	f_{c0} [N/mm ²]	G_{fc} [N/mm]	ψ [°]	η [s]	χ
joints	0,25	0,018	10,5	∞	0	30	0,01

5 CONCLUSIONS

In this paper, a mesoscopic masonry model is developed in which joints are modelled by weak discontinuities. The discontinuities are incorporated using the Generalized Finite Element Method. A modified Drucker-Prager model is used to describe the failure of the mortar joints, whereas the stone behaviour remains linear elastic. A Perzyna viscoplastic model is employed as a regularisation technique. Special attention was given to the algorithmic aspects of the model. A three-point bending test and a shear wall test showed that the presented method leads to realistic load capacities and failure patterns. In the example of the shear wall test, the results showed good agreement with those of previous research work, although the modelling approaches differ.

ACKNOWLEDGMENT

The support of this research by the Bijzonder Onderzoeksfonds Doctoral Funding program of Hasselt University (BOF-DOC) is gratefully acknowledged.

REFERENCES

- [1] Lourenço, P.B. *Computational Strategies for Masonry Structures*. PhD Thesis, (1996). Technische Universiteit Delft.
- [2] Alfaite, J.V. and de Almeida, J.R. Modelling Discrete Cracking on Masonry Walls. *Masonry International* (2004) **17**(2): 83–93.
- [3] Belytschko, T. and Black, T. Elastic Crack Growth in Finite Elements with Minimal Remeshing. *Int. J. Num. Meth. Engng.* (1999) **45**(5): 601–620.
- [4] Wells, G.N. and Sluys, L.J. A New Method for Modelling Cohesive Cracks Using Finite Elements. *Int. J. Num. Meth. Engng.* (2001) **50**(12): 2667–2682.
- [5] De Proft, K. *A Combined Experimental-Computational Study to Discrete Fracture of Brittle Materials*. PhD Thesis, (2003). Vrije Universiteit Brussel.
- [6] De Proft, K., Heyens, K. and Sluys, L.J. Mesoscopic Modelling of Masonry Failure. *Proceedings of the ICE - Engineering and Computational Mechanics* (2010) **164**(EM1): 41–46.

- [7] Belytschko, T., Fish, J. and Engelman, B.E. A Finite-Element with Embedded Localization Zones. *Comput. Meth. Appl. Mech. Eng.* (1988) **70**(1): 59–89.
- [8] Sluys, L.J. and Berends, A.H. Discontinuous Failure Analysis for Mode-I and Mode-II Localization Problems. *Int. J. Solids Structures* (1998) **35**(31-32): 4257–4274.
- [9] Jirásek, M. Comparative Study on Finite Elements with Embedded Discontinuities. *Comput. Meth. Appl. Mech. Eng.* (2000) **188**(1-3): 307–330.
- [10] Oliver, J., Cervera, M. and Manzoli, O. Strong Discontinuities and Continuum Plasticity Models: the Strong Discontinuity Approach. *Int. J. Plast.* (1999) **15**(3): 319–351.
- [11] Simone, A., Duarte, C.A. and Van der Giessen, E. A Generalized Finite Element Method for Polycrystals with Discontinuous Grain Boundaries. *Int. J. Num. Meth. Engng.* (2006) **67**(8): 1122–1145.
- [12] Feenstra, P.H. Implementing an isotropic damage model in Diana. Use-case for the user-supplied subroutine usrmat. *Proceeding of the Third DIANA World Conference* (2002).
- [13] Massart, T.J., Peerlings, R.H.J. and Geers, M.G.D. Mesoscopic Modeling of Failure and Damage-induced Anisotropy in Brick Masonry. *European Journal of Mechanics a-Solids* (2004) **23**(5): 719–735.
- [14] de Souza Neto, E.A., Perić, D. and Owen, D.R.J. *Computational Methods For Plasticity, Theory and Applications*. John Wiley & Sons Ltd, Chichester, (2008).
- [15] Wells, G.N. *Discontinuous Modelling of Strain Localisation and Failure*. PhD Thesis, (2001). Technische Universiteit Delft.
- [16] Sluys, L.J. *Wave Propagation, Localisation and Dispersion in Softening Solids*. PhD Thesis, (1992). Technische Universiteit Delft.
- [17] Perzyna, P. Fundamental Problems in Viscoplasticity. *Recent Advances in Applied Mechanics*. Academic Press, New York, (1966) **9**: 243–377.
- [18] de Borst, R. The Zero-Normal-Stress Condition in Plane-Stress and Shell Elastoplasticity. *Comm. Appl. Numer. Meth.* (1991) **7**(1): 29–33.
- [19] Chaimoon, K. and Attard, M.N. Experimental and Numerical Investigation of Masonry under Three-Point Bending (In-Plane). *Eng. Struct.* (2009) **31**(1): 103–112.
- [20] Raijmakers, T.M.J. and Vermeltvoort, A.T. *Deformation Controlled Tests in Masonry Shear Walls*. Report B-92-1156, (1992). TNO Bouw, Delft.